Collective dynamics of self-propelled sphere-dimer motors

Snigdha Thakur*
Department of Physics, Indian Institute of Science Education and Research Bhopal, Bhopal, MP-462023, India

Raymond Kapral†
Chemical Physics Theory Group, Department of Chemistry, University of Toronto, Toronto, Ontario M5S 3H6, Canada
(Received 2 November 2011; revised manuscript received 31 January 2012; published 29 February 2012)

The collective dynamics of ensembles of chemically powered sphere dimer motors is investigated. Sphere dimers are self-propelled nanomotors built from linked catalytic and noncatalytic spheres. They consume fuel in the environment and utilize the resulting self-generated concentration gradients to produce directed motion along their internuclear axes. In collections of such motors, the individual motors interact through forces that arise from concentration gradients, hydrodynamic coupling, and direct intermolecular forces. Under nonequilibrium conditions it is found that the sphere dimer motors self-assemble into transient aggregates with distinctive structural correlations and exhibit swarming where the aggregates propagate through the system. The mean square displacement of a dimer motor in the ensemble displays short-time ballistic and long-time diffusive regimes and, for ensembles containing many motors, an increasingly prominent intermediate regime. The self-diffusion coefficient of a motor in a many-motor system behaves differently from that of an isolated motor, and the decay of orientational correlations is a nonmonotonic function of the number of motors. The results presented here illustrate the phenomena to be expected in applications, such as cargo transport, where many motors may act in consort.

DOI: 10.1103/PhysRevE.85.026121 PACS number(s): 05.65.+b, 87.18.Gh

I. INTRODUCTION

Active particles that utilize energy sources to effect motion arise in many contexts and endow the systems in which they operate with special properties. Biological examples include molecular motors such as kinesin and myosin that are propelled by mechanical forces derived from the chemical energy released during the hydrolysis of adenosine triphosphate [1–3], and bacteria that swim by executing nonreciprocal motions [4,5]. Synthetic molecular motors that use various types of energy for propulsion and move in viscous media as a result of conformational changes or chemical gradients have been constructed and studied both experimentally and theoretically [6–17].

Active particles can communicate with each other through a number of different mechanisms, including direct intermolecular potential interactions among neighbors, hydrodynamic interactions, chemical gradients, etc. The collective dynamics of systems containing many such interacting active particles have properties that differ from those of systems of comprising inactive particles. This behavior is manifested in the familiar examples of the flocking of birds and the schooling of fish [18,19]. There have been extensive studies that have modeled and characterized the generic features that give rise to such dynamics [20–25]. Suspensions of active particles have been shown to exhibit features such as swarming, giant number fluctuations, and various types of pattern formation [24,26,27]. The dynamics of suspensions of swimming particles in confined geometries have also been investigated [28,29]. In the biological realm, the collective behavior of molecular motors plays an important role in phenomena including intracellular, intraflagellar, and axonal transport [30]. The collective motion of bacteria leads to rippling patterns [31–33], induced flow patterns, swarming, and anomalous density fluctuations [34–38]. There have also been experimental studies of the collective dynamics of synthetic chemically powered motors. Self-assembly of chemically active Janus colloidal particles [39] and schooling of light-powered micromotors [40] have been observed and studied. Studies of the interactions of pairs [41] of three-bead swimmers [42] and interactions between spherical and ellipsoidal swimmers [43] whose motions are coupled by hydrodynamic interactions have been carried out. The dynamics of pairs of sphere dimer motors have been studied [16].

The collective dynamics of chemically powered sphere dimer motors is investigated in this paper. These self-propelled nanomotors comprise catalytic and noncatalytic spheres (Pt and Silica spheres, respectively, in the laboratory realizations of such motors [13]) that consume fuel in the environment and make use of the self-generated concentration gradients to effect directed motion. The collective motions of these namomotors described below arise from a combination of interactions due to chemical gradients, hydrodynamic coupling, and repulsive short-range intermolecular interactions. In Sec. III we give an overview of the collective phenomena observed in simulations of ensembles of sphere dimer motors. A quantitative characterization of the dynamics is presented in Sec. IV where the mean squared displacement, dimer diffusion coefficient, and orientational correlation functions are discussed. The conclusions of the investigation are given in Sec. V.

II. MESOSCOPIC DYNAMICAL MODEL

We consider the dynamics of ensembles of N_D sphere dimer motors. Each nanodimer consists of linked catalytic C and

*sthakur@iiserbhopal.ac.in
†rkapral@chem.utoronto.ca

noncatalytic N spherical monomers with a fixed internuclear separation [14,15,44]. Rather than using an intermolecular potential to bind the spheres in the dimer, the dimer internuclear distance is fixed at R by a holonomic constraint in the dynamics. The dimers are confined in a three-dimensional slab geometry between two parallel walls at a distance L_z apart, perpendicular to the z direction of the system. The dimer motors interact with the walls through dimer-monomer-wall, 9-3-Lennard-Jones (LJ) interactions,

$$V_{LJ}^{93}(r) = 4\epsilon_{\rm w}\left[\left(\frac{\sigma_{\rm w}}{r}\right)^9 - \left(\frac{\sigma_{\rm w}}{r}\right)^3\right]. \quad (1)$$

Here $\epsilon_{\rm w}$ and $\sigma_{\rm w}$ are the wall energy and distance parameters. We take $\sigma_{\rm w} = L_z/2$. The existence of these monomer wall interactions leads to dimer motion that deviates little from the xy plane in the center of the slab [45]. As a result, the orientational and translational motion of the nanodimers along z is suppressed and the collective motion easier to visualize and analyze. The simulation box has dimensions $L_x = L_y$ in the x and y directions, and periodic boundary conditions were employed in these directions.

The system also contains $N_s = N_A + N_B$ pointlike A and B solvent molecules with identical masses m. These solvent molecules interact with walls through bounce-back collisions that reverse their velocity on collision with the walls. The solvent molecules interact with the dimer monomers through repulsive LJ interactions of the form

$$V_{\alpha S}(r) = 4\epsilon\left[(\sigma/r)^{12} - (\sigma/r)^6 + \tfrac{1}{4}\right]\theta(r_c - r), \quad (2)$$

where $\theta(x)$ is the Heaviside function and $r_c = 2^{1/6}\sigma$ is the cutoff distance. We use the notation $V_{\alpha S}$, where $S = C, N$ and $\alpha = A, B$ to denote various interactions between solvent and dimer monomers. In particular, we take $V_{AC} = V_{BC} = V_{AN}$, which are characterized by the energy and distance parameters $\epsilon = \epsilon_A$ and $\sigma = \sigma_S$, respectively; however, interactions between the N sphere and B molecules, V_{BN}, have energy parameter $\epsilon = \epsilon_B$. Hence the B molecules produced in the reaction on the catalytic sphere react differently with the C and N monomers [14,15].

In the multidimer simulations, the monomers in different dimers also interact through repulsive LJ potentials, so that there are no cohesive intermolecular forces between dimers. The repulsive LJ potentials between monomers in different dimers have energy parameter ϵ_D and distance parameter $\sigma_D = \sigma_{S_\nu} + \sigma_{S'_\nu} + \delta_D$. We let $S_\nu, S'_\nu = C_\nu, N_\nu$ and $\nu = 1, \ldots, N_D$ denote the dimers in the system. The symbols C_ν and N_ν denote the catalytic and noncatalytic monomers of dimer ν.

Nonreactive collisions of A and B molecules take place with the noncatalytic sphere. An irreversible chemical reaction [46] $A + C \to B + C$ occurs at the catalytic monomer C. To maintain the system in a nonequilibrium steady state, product B molecules are removed in the vicinity of the confining walls and reactant A molecules are inserted in a manner that satisfies mass, momentum, and energy conservation. The slab geometry provides a convenient way to implement the nonequilibrium steady state. The sphere dimers require a supply of fuel for their motion. Often experimental realizations of far-from-equilibrium conditions in reaction-diffusion systems using continuously fed unstirred reactors allow for fluxes of reagents in slab geometries to effectively introduce and remove chemical species under conditions with small chemical gradients normal to the walls. Likewise, in the slab geometry employed here fuel can easily reach the motors. In other three-dimensional geometries the interior of the system may be quickly depleted of fuel and remain screened by other motors; thus some motors will cease to move giving rise to other types of collective behavior.

The time evolution of the system is carried out using a mesoscopic hybrid molecular dynamics–multiparticle collision dynamics (MD-MPC) scheme. The solvent molecules interact among themselves by multiparticle collision (MPC) dynamics [47–51], which consists of a streaming step and a collision step. In the steaming step, the dynamics of both solvent and monomer particles are governed by Newton's equations of motion. In the collision steps, which occur at time intervals τ, the pointlike solvent particles are sorted into cubic cells with lattice size a_0. Multiparticle collisions among the solvent molecules are performed independently in each cell, and the postcollision velocity of solvent particle i in cell ξ is given by $\mathbf{v}'_i = \mathbf{V}_\xi + \hat{\omega}_\xi(\mathbf{v}_i - \mathbf{V}_\xi)$, where $\hat{\omega}_\xi$ is a rotation matrix and $\mathbf{V}_\xi$ is the center-of-mass velocity of that cell. The dynamics is microcanonical, satisfies mass, momentum, and energy conservation, and also preserves phase space volumes. As a result, hydrodynamic interactions both among dimer monomers [52] and with the walls [53] are automatically taken into account. In some cases, in order to assess the importance of hydrodynamic interactions on the collective dynamics, the dynamical simulation algorithm was modified [51] by replacing the multiparticle collision step with choosing the solvent particle postcollision velocities in a cell from a Maxwell-Boltzmann distribution. In this case solvent hydrodynamical correlations are destroyed and momentum and energy are no longer locally conserved. Hence hydrodynamic interactions are absent for such dynamics, although the intermolecular potential functions are unchanged.

In the simulations described below, all quantities are reported in dimensionless LJ units based on energy ϵ_A, mass m_A, and distance σ_A parameters. The masses of both A and B species are $m = 1$ and the masses of the C and N spheres were adjusted according to their diameters, $d_C = 2\sigma_C$ and $d_N = 2\sigma_N$, to ensure density matching between monomers and solvent. The internuclear separation between C and N spheres in each dimer was fixed at $R = (d_C + d_N)/2 + \delta$, with $\delta = 0.8$, by a holonomic constraint. The system temperature was $T = 1/6$. The MD step, which was used to integrate Newton's equations of motion with the velocity Verlet algorithm was $\Delta t = 0.01$, while the MPC time was $\tau = 0.5$. The LJ parameters for solvent-nanodimer interactions were chosen to be $\epsilon_A = 1.0$ and $\epsilon_B = 0.1$. The interaction energy between monomers in different dimers was taken to be $\epsilon_D = 5.0$ and δ_D in the expression for the distance parameter σ_D was $\delta_D = 0.2$.[1] The wall interaction parameters were taken to be $\sigma_{\rm w} = L_z/2$ and $\epsilon_{\rm w} = 1.0$.

[1]For these energy parameters, when two dimers collide they do not form bound pairs as a result of solvent depletion forces and separate after collision [16]. This choice of energy parameter allows us to focus on structures arising from many-body collective effects.

The simulation box dimensions were $L_x = 65$, $L_y = 65$, and $L_z = 20$. The cell size for MPC solvent dynamics was $a_0 = 1$ and the MPC rotation angle was fixed at $\alpha = 90^\circ$. The total number of solvent molecules in the box was 760 500 giving an average density of $n_0 \approx 9$ solvent particles/cell.

III. SPHERE DIMER COLLECTIVE DYNAMICS

Previously we investigated the dynamics of pairs of sphere dimer motors which were initially targeted toward each other [16]. Depending on the interaction strength and ratio of catalytic to noncatalytic sphere diameters, either bound pairs with various characteristics that arose as a result of solvent depletion forces or scattering events that did not give rise to long-lived bound-pair formation were observed. The dynamical behavior of ensembles of sphere dimer motors considered in this paper was studied in parameter regimes where isolated binary collisions do not lead to long-lived bound-pair formation (see Fig. 1 of Ref. [16]). In particular, the energy parameter in the repulsive LJ potential that characterizes interactions between monomer on different dimers was chosen to be large ($\epsilon_D = 5$) so that, in the absence of any other effects due to concentration gradients or hydrodynamic interactions, sphere dimers strongly repel one another and cannot approach closely for depletion forces to play a role. Thus we are able to focus on structures that arise as a result of collective behavior among the dimers in the ensemble.

A. Overview of structure and dynamics

We begin with a study of the dynamics of motors with catalytic and noncatalytic monomer diameters of $d_C = 4$ and $d_N = 8$, respectively. Potential energy parameters are chosen so that an isolated sphere dimer motor moves in a direction with the catalytic sphere at the motor head. Figure 1 shows instantaneous configurations that arise in the course of the evolution of a small ensemble of $N_D = 5$ dimers. (A video of the dynamics can be found in the Supplemental Material, Movie 1 [54].) Transient but long-lived clusters of dimer motors self-assemble and propagate as a unit. Collisions of such clusters with other clusters or single motors lead to either self assembly or fragmentation of the clusters. Thermal fluctuations can also lead to cluster fragmentation. The figure also shows the B particle density field, which is produced by chemical reactions at the surfaces of the catalytic spheres. One can see how the concentration fields arising from individual dimers combine to produce much more complex concentration patterns, which then influence the collective dimer motion.

Our mesoscopic particle-based description of the dynamics accounts for both hydrodynamic coupling among the motors which exists in the slab geometry, as well as motion induced by gradients of chemical species arising from the reactions at the catalytic monomers. Both of these effects play effective roles in determining the character of the collective motion. Chemical gradients play an especially important role in the self-assembly process and in the resulting cluster dynamics. The self-generated concentration gradient arising from reaction at the C surface is an essential element in the dimer propulsion mechanism [14]. The long-range inhomogeneous concentration field produced by motors in the vicinity of a given motor will influence its propulsion properties, since the motor will respond its local concentration gradient as well as that of neighboring motors. The dimer motors will move up the gradient and tend to be propelled toward neighboring motors. Once two or more motors approach closely, they typically tend to align, since motor configurations with the N end toward the C end of a neighboring motor will result in a small concentration gradient across the N monomer. Configurations with the majority of motors aligned in a given direction will undergo self-propelled motion in that direction, as seen in Fig. 1, until the aggregate fragments as a result of fluctuations or collisions with other motors or aggregates.

Configurations extracted from the dynamics of an ensemble of $N_D = 10$ dimers are shown in Fig. 2. (See Movie 2 in the Supplemental Material [54].) The nature of the collective behavior is more evident in this larger ensemble. One can see chains of oriented, propagating motors and larger propagating clusters that exhibit swarminglike behavior. One can also see configurations where the smaller catalytic spheres tend to be surrounded by the larger noncatalytic spheres, consistent with the structure dictated by the motion induced by the chemical gradients and packing of the dimers. For systems with $N_D = 5$ and 10 the dimer area fractions are quite small, $\phi = 0.07$ and 0.14, respectively, so the assembly into clusters cannot be attributed to simple packing in the volume. As can be seen in Movie 3 in the Supplemental Material [54], when chemical reactions do not take place at the catalytic spheres, clustering does not occur.

Investigations of ensembles of simple dumbbell swimmers composed of two beads have been carried out in confined slab geometries where the beads in the swimmer act as point sources to determine the fluid velocity from the solution of Stokes' equation. The role of hydrodynamic interactions on the collective dynamics has been investigated and the results of simulations have shown that such interactions can lead to complex behavior [28,29]. Confinement also leads to migration of particles, which gives rise to density profiles that depend on the swimmer volume fraction. The walls also modify the hydrodynamic interactions among particles and between the wall and the particles since the finite distance to the walls provides a cutoff for the long range hydrodynamic fields. Our particle-based simulations, where finite-size dimers

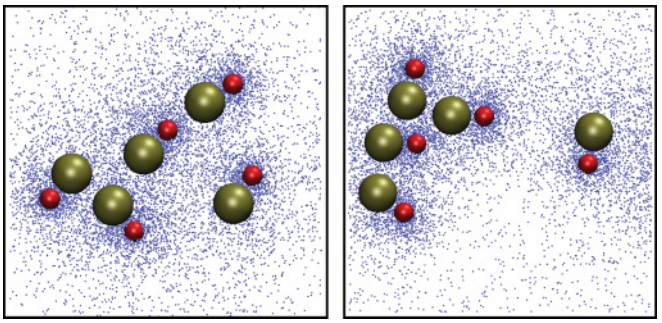

FIG. 1. (Color online) Two instantaneous configurations of a small ensemble of five sphere dimers showing the formation of transient propagating clusters. The concentration field of the pointlike B particles is also shown. The dimer monomers have diameters of $d_C = 4$ and $d_N = 8$.

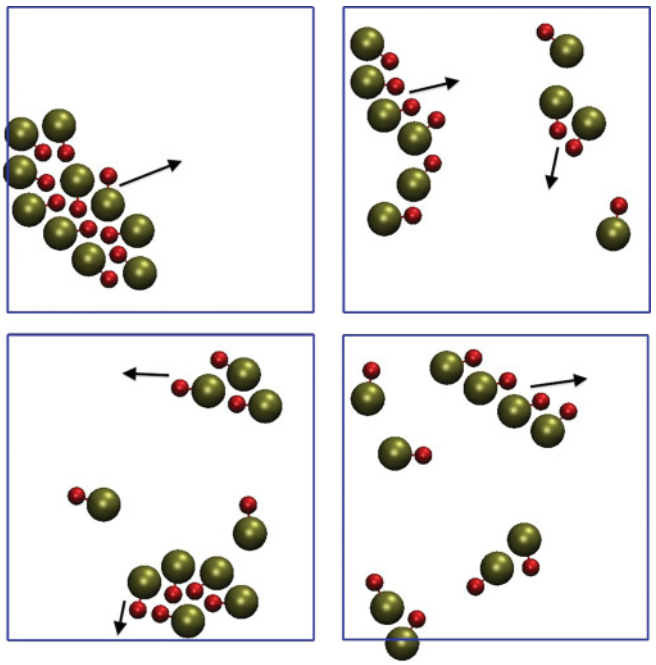

FIG. 2. (Color online) Instantaneous configurations observed in the dynamical evolution of an ensemble of $N_D = 10$ dimer motors with monomer diameters of $d_C = 4$ and $d_N = 8$.

interact with a solvent described at a coarse-grained molecular level, account for any modifications of the hydrodynamic interactions due to the presence of the walls since all conservation laws are preserved. The dimer-wall interactions [Eq. (1)] introduced in our simulations serve to restrict the dynamics close to the midplane in the slab. Even in this situation, given the finite sizes of the monomers in the dimers and the separation between the walls, hydrodynamic effects are expected to be modified from their infinite system size analogs. The main feature that distinguishes our studies of self-propelled particles in slab geometries from these other investigations is the presence of chemical gradients that occur as a result of reactions on the catalytic spheres. As argued above, the existence of such gradients can explain

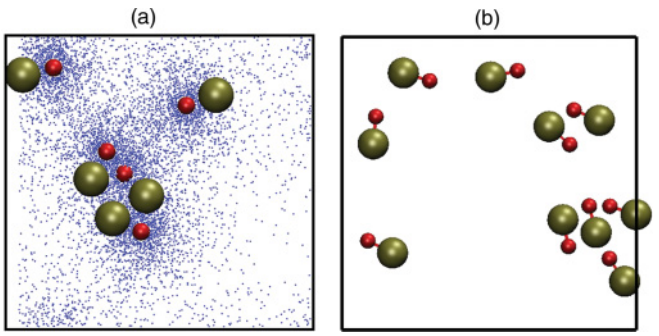

FIG. 3. (Color online) (a) Instantaneous configurations of an ensemble of five sphere dimers showing the formation of transient clusters even in the absence of hydrodynamic interactions. The concentration field of the pointlike B particles is also shown. (b) Ensemble of ten dimers showing the cluster formation in absence of hydrodynamic interactions. The dimer monomers have diameters of $d_C = 4$ and $d_N = 8$.

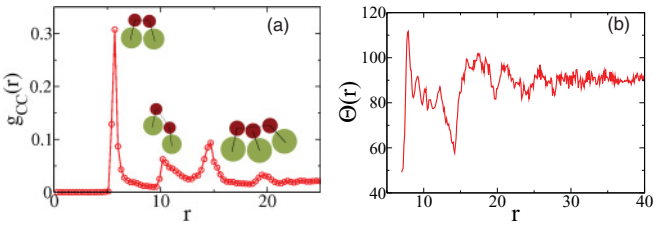

FIG. 4. (Color online) (a) CC radial distribution function for a system with $d_C = 4.0$ and $d_N = 8.0$. The insets show cluster configurations that contribute to the peaks in the distribution function. Distances corresponding to various peaks are shown as dashed lines in the corresponding configurations. (b) Average angle (in degrees) between unit vectors $\hat{\mathbf{z}}_\nu$ of dimers whose centers of mass are a distance r apart for a system having $N_D = 10$ dimers with $d_C = 4.0$ and $d_N = 8.0$.

the clustering phenomena observed in the simulations. To confirm this point, using the simulation scheme described in Sec. II, we carried out simulations of the dynamics where hydrodynamic interactions were absent. Even in the absence of hydrodynamic interactions propagating long-lived clusters of dimers are formed (see Fig. 3); thus while hydrodynamic interactions are certainly important and on their own can lead to complex collective effects, the chemical gradients in our system likely play a dominant role in determining the nature of the observed collective dynamics since the phenomena we observe occur in absence of hydrodynamic coupling.

The characteristic structural features that occur in the course of the dynamics of the ensemble can be identified in the steady-state radial distribution functions in the plane of the motion. Figure 4(a) shows a plot of the catalytic-catalytic (CC) radial distribution function,

$$g_{CC}(r) = \frac{1}{2\pi r n_C} \left\langle \sum_{j<i=1}^{N_C} \delta(|\mathbf{r}_{Ci} - \mathbf{r}_{Cj}| - r) \right\rangle, \qquad (3)$$

where $\mathbf{r}_{Ci}$ is the position of catalytic monomer i, N_C is the number of catalytic monomers, n_c is the number density of catalytic monomers and the angle brackets denote an average over time and realizations. There are well defined peaks in this function that can be identified with the configurations seen in the instantaneous configurations in the previous figures, indicating that these structures persist throughout the course of the steady-state evolution. Similar correlations are observed in the other monomer-monomer radial distribution functions.

The orientational ordering in the system can be gauged by the average angle $\Theta(r)$ between dimers separated by a center of mass distance of r:

$$\Theta(r) = \left\langle \sum_{\nu'<\nu=1}^{N_D} \arccos\left[\hat{\mathbf{z}}_\nu(\mathbf{R}_\nu) \cdot \hat{\mathbf{z}}_{\nu'}(\mathbf{R}_{\nu'})\right] \delta(R_{\nu\nu'} - r) \right\rangle, \qquad (4)$$

where the angular brackets again signify an average over time and over realizations. Here, $\hat{\mathbf{z}}_\nu$ is the unit vector along the dimer bond (directed from N to C), $\mathbf{R}_\nu$ is the center of mass of dimer ν, and $R_{\nu\nu'} = |\mathbf{R}_\nu - \mathbf{R}_{\nu'}|$. From this definition it follows that parallel and antiparallel alignments of dimers are characterized by $\Theta = 0$ and π, respectively, while perpendicular orientations correspond to $\pi/2$. If the dimer orientations are uncorrelated, the average angle will also be $\Theta = \pi/2$. This function is

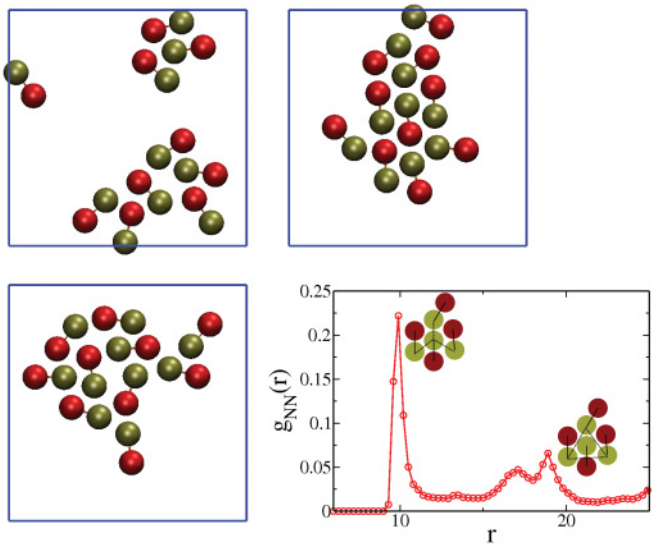

FIG. 5. (Color online) Instantaneous configurations for a system of $N_D = 10$ dimers with monomers of equal size $d_C = d_N = 8$. The last panel plots the noncatalytic-noncatalytic (NN) radial distribution function, $g_{NN}(r)$ versus r. The area fraction of dimers is $\phi = 0.23$.

plotted in Fig. 4(b) for a system with $N_D = 10$. At small separations, $r < 10.0$, one can see evidence for nearly parallel and antiparallel alignments of nearest neighbor dimers. The dip in $\Theta(r)$ at $r \approx 15.0$ is due to parallel alignment of next nearest neighbor dimers. At intermediate values of r, $10.0 < r < 15.0$, $\Theta(r) \approx \pi/2$, signaling the appearance of perpendicular configurations that can be seen in Fig. 2. For large separation distances $\Theta \approx \pi/2$ again, consistent with a lack of angular correlation between widely separated dimers.

Thus far we have considered sphere dimers where the C sphere is smaller than the N sphere. Dimer geometry is also an important factor in determining the nature of the self-assembled structures. Instantaneous cluster configurations for dimers comprising monomers of equal size ($d_C = d_N = 8$) are shown in Fig. 5. Hexagonal-like ordering is seen in the interior of the larger clusters and such structure is confirmed in the radial distribution function plot also shown in this figure. Here the monomer-monomer radial distribution function g_{NN} is for the noncatalytic monomers.

IV. DYNAMICAL PROPERTIES

An isolated sphere dimer undergoes self-propelled motion in the direction of its internuclear axis with average velocity $\langle V_z \rangle$; however, such nanomotors are also subject to strong thermal fluctuations that lead to a distribution of propagation velocities. This distribution has been shown [14,15,44] to be closely approximated by a Boltzmann distribution with mean $\langle V_z \rangle$. If an ensemble of interacting motors is considered, the peak of the distribution shifts to smaller velocities and exhibits a long tail toward smaller or even negative velocities. As the number of motors in the ensemble increases further, the peak in the distribution continues to shift to smaller velocities and closely approaches zero, but now the distribution possesses a long tail toward higher velocities. The structure of the high-velocity shoulder of this distribution suggests that there may be

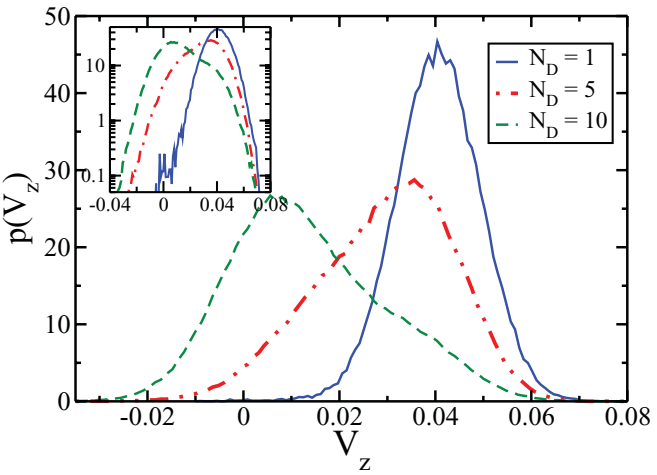

FIG. 6. (Color online) Plots of $p(V_z)$, the unnormalized probability density of V_z, for $N_D = 1$, 5, and 10 dimers. The monomers in the dimers have diameters $d_C = 4$ and $d_N = 8$. Inset shows the same data in lin-log scale.

underlying bimodal structure, possibly arising from different cluster configurations that contribute to the ensemble. These trends are seen in Fig. 6, which displays the (unnormalized) velocity distributions, $p(V_z)$, for systems with $N_D = 1$, 5, and 10 dimers. The average velocities are given in Table I. While the average and peak dimer velocities are the same for $N_D = 1$ and 3, they differ considerably for larger ensembles. These results are consistent with the existence of the transient self-assembled structures discussed previously. Clusters of dimers move with varying velocities. Dimers within such clusters move with the speed of the cluster and may have orientations at angles different from their directed motion. Such effects are responsible for the wide dispersion of V_z velocities.

In addition to directed motion, isolated dimers undergo orientational Brownian motion characterized by the orientational relaxation time τ_R, which can be obtained from the decay of the orientational autocorrelation function. Similarly, for a system of N_D dimers we can define the orientational autocorrelation function as

$$C_\theta(t; N_D) = N_D^{-1} \sum_{\nu=1}^{N_D} \langle \hat{\mathbf{z}}_\nu(t) \cdot \hat{\mathbf{z}}_\nu(0) \rangle \sim e^{t/\tau_R(N_D)}, \qquad (5)$$

where again $\hat{\mathbf{z}}_\nu$ is the unit vector along the bond of dimer ν. The relaxation time extracted from the decay of this correlation function, $\tau_R(N_D)$, is not a monotonic function of N_D. We find $\tau_R(1) > \tau_R(10) > \tau_R(5)$ (see Table I and Fig. 7). For small N_D, dimer-dimer collisions provide an additional reorientation

TABLE I. Various dynamical properties for several ensemble sizes N_D. The area fractions ϕ for the systems are also listed.

N_D	ϕ	$\langle V_z \rangle$	V_p	τ_R	D	t_c
1	0.014	0.0367	0.0367	3550	2.25	6451
3	0.042	0.0346	0.0365	1350	0.72	2400
5	0.070	0.0286	0.0350	1000	0.45	2150
8	0.112	0.0198	0.0160	1250	0.28	2000
10	0.140	0.0190	0.0075	1440	0.17	1710

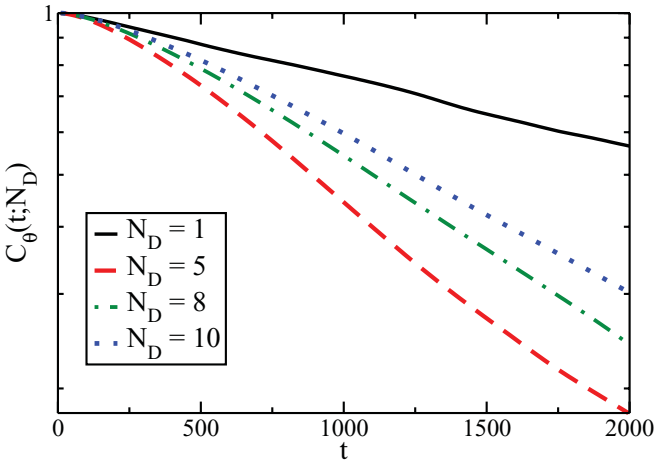

FIG. 7. (Color online) The orientational autocorrelation function for $N_D = 1$ (solid line), $N_D = 5$ (dashed line), $N_D = 8$ (dotted-dashed line) and $N_D = 10$ (dotted line) dimers. The catalytic and noncatalytic monomers have dimeters $d_C = 4$ and $d_N = 8$, respectively.

mechanism that gives rise to reorientation times that are shorter than those due to Brownian motion of single dimer. As the number of dimers in the ensemble increases, cluster configurations exist with dimers locked for long times in specific orientations within the clusters, leading to an increase in the reorientation time.

New dynamical features due to correlations among dimers in the ensemble are also reflected in the nature of the dimer mean square displacement (MSD),

$$\Delta L^2(t) = N_D^{-1} \sum_{\nu=1}^{N_D} \langle |\mathbf{R}_\nu(t) - \mathbf{R}_\nu(0)|^2 \rangle, \tag{6}$$

and the dimer diffusion coefficient defined by $D = \lim_{t\to\infty} \Delta L^2(t)/4t$. (We use the two-dimensional form since the motion is largely confined to the xy plane lying at the midpoint between the walls.) The form of the MSD and the diffusion coefficient have been analyzed in some detail for a single chemically powered particle by Golestanian [55].

A number of time scales are relevant for the analysis. For our purposes important characteristic times are $\tau_D = R_d^2/D_s$, the time that gauges how long it takes solvent molecules to diffuse a distance equal to the dimer size R_d, where D_s is the diffusion coefficient of solvent molecules, and τ_R, which was discussed earlier and is the time it takes for the dimer orientational autocorrelation, $\langle \hat{\mathbf{z}}(t) \cdot \hat{\mathbf{z}}(0) \rangle \sim e^{-t/\tau_R}$, to decay. The solvent transport coefficients can be computed analytically for MPC dynamics. The expression for the solvent diffusion coefficient is

$$D_s = \frac{k_B T \tau}{2m} \left[\frac{3\gamma}{(\gamma - 1 + e^{-\gamma})(1 - \cos\alpha)} - 1 \right], \tag{7}$$

where γ is the average number of solvent particles per cell and τ is the MPC collision time. Considering sphere dimers with $d_C = 4$ and $d_N = 8$ and evaluating the transport coefficient expression for the parameters given in Sec. II, we have $\tau_D \approx 180$ and $\tau_R = 3550$, taking the effective dimer size to be

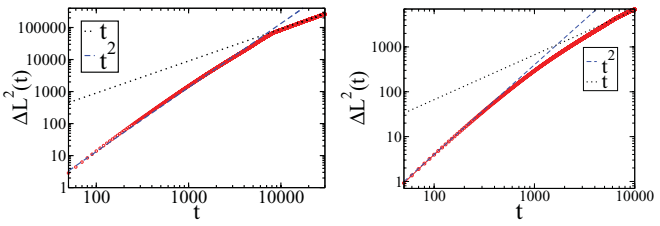

FIG. 8. (Color online) Mean square displacement $\Delta L^2(t)$ for a nanodimer showing ballistic motion $\sim t^2$ at short times and diffusive motion $\sim t$ at long times. Left: MSD for a system containing a single dimer. Right: MSD for a system containing ten dimers.

$R_d = 4.2$ obtained from the total volume of the C and N spheres. Thus $\tau_D \ll \tau_R$.

For short times ($t \ll \tau_D$) there is a ballistic regime where $\Delta L^2(t) \sim \langle V_z \rangle^2 t^2$. (The correction term proportional to the prefactor of t^2, which is proportional to τ_D/τ_R, is negligible.) For very short times there is an inertial regime where $\Delta L^2(t) \sim \overline{\delta V^2} t^2$, with $\overline{\delta V^2} = 3k_BT/M$ the mean thermal squared speed of the dimer with $\delta\mathbf{V} = \mathbf{V} - \hat{\mathbf{z}}V_z$. Since $3k_BT/M \ll \langle V_z \rangle^2$, this contribution to the t^2 coefficient is masked by the $\langle V_z \rangle^2$ component. For long times, $t \gg \tau_R$, the MSD is a linear function of time, $\Delta L^2(t) \sim 4(D_0 + \langle V_z \rangle^2 \tau_R/2)t$, which can be used to find the diffusion coefficient of the self-propelled sphere dimer: $D = D_0 + \langle V_z \rangle^2 \tau_R/2$. Here D_0 is the diffusion coefficient of the dimer when there is no chemically powered self-propulsion, which in our case is 0.003.

The MSD for a single motor plotted in Fig. 8 (left) shows the ballistic and diffusive regimes. The straight lines in this graph are plots of the theoretical short and long time MSD expressions given above, with coefficients determined from the independently measured average dimer propagation velocity $\langle V_z \rangle$ and reorientation time τ_R. These asymptotic expressions are consistent with the MSD simulation data. The time that characterizes the crossover from the ballistic to diffusive regimes, t_c, may be determined from the intersection of the straight line segments that correspond to the ballistic and diffusive regimes in the log-log plot. We find $t_c(1) = 6451$ for a system containing a single dimer.

At intermediate times, $\tau_D \ll t \ll \tau_R$, the MSD is predicted [55] to behave as $\Delta L^2(t) \sim \langle V_n \rangle^2 (t^2 + \frac{8\tau_D^{3/2}}{3\sqrt{\pi}\tau_R} t^{3/2})$. The coefficient of $t^{3/2}$ is small and this behavior is difficult to detect in the figure.

Given this description of MSD for a single self-propelled dimer, we now study this quantity for an ensemble of sphere dimers. Figure 8 (right) shows the MSD for a system with 10 dimers. The graph clearly exhibits the ballistic and diffusive regimes. The crossover time is $t_c(10) = 1710$, much shorter than that for a single dimer. Comparison of the left and right panels of Fig. 8 shows that a regime, intermediate between the ballistic and diffusive regimes, grows in size as N_D increases. Similar behavior of the MSD has been observed for ensembles of simple dumbbell swimmers in slab geometry whose collective behavior is controlled by hydrodynamic interactions [28]. In particular, short time ballistic and long time diffusive regimes were found and, as the number of swimmers increased, an intermediate regime of anomalous diffusion was seen that extended over more than a decade in time.

The data presented in Table I summarize how important dynamical properties vary with N_D. As evident in the table, both D and τ_R vary strongly with N_D. The dimer diffusion coefficient, determined from the linear behavior of the MSD, is found to decrease with increasing N_D as might be expected; however, as discussed earlier, τ_R is a nonmonotonic function of N_D. Hence the relation between D and τ_R, $D = D_0 + \langle V_z \rangle^2 \tau_R/2$, which applies for a single dimer, is no longer valid in a multidimer system.

The collective dynamics of the sphere dimer motors should exhibit many of the features that have been found to exist in collections of active particles. Although the intermolecular potentials through which the sphere dimers interact are repulsive so that there are no direct cohesive forces, the motions of the dimers are also coupled through forces arising from chemical gradients and hydrodynamic coupling through solvent viscous modes. Consequently, the dynamical model that underlies the behavior described above is more complicated than that in some simple models that have been used to investigate the properties of the collective dynamics of active particles [20–22]. Nevertheless, certain features, such as clustering and swarming, have analogs in our sphere dimer system. A complete quantitative investigation of properties such as the possible existence of superdiffusion and the exponents that characterize it [56,57], the existence of giant number fluctuations [58], and the possibility of nonequilibrium phase transitions [21,22] will require much larger ensembles and more extensive simulations than those considered here and are topics of future research. However, it is worth noting that our simulations of small ensembles of sphere dimers point to the existence of some other phenomena. For example, the transient formation and breakup of clusters leads to large density fluctuations in the system. In addition, as the number of dimers increases, the MSD exhibits a transition region between the ballistic and diffusive regimes that grows in size and, from the limited length of this intermediate regime in small-ensemble systems, appears to scale as a power law, $\mathrm{MSD}(t) \sim t^{\nu}$, with $\nu \approx 3/2$. Such superdiffusive power-law behavior has been observed in active systems in a number of different contexts. Experimental studies [59] of the MSD of beads in a medium containing active bacteria has a superdiffusive power law behavior for short times with an exponent $3/2 < \nu < 2$. Investigations of Vicsek-style models have shown the existence of a phase transition to a regime where there are propagating high density regions with complex internal structure in the system [21,22]. The MSD transverse to the propagation direction behaves as a power law with $\nu = 4/3$ [56]. In the isotropic transition regime where there is no global order, the MSD exhibits a power law scaling with $\nu = 5/3$ [57]. The origin of this behavior has been attributed to the fact that particles have ballistic trajectory segments when they lie within a coherently moving cluster and normal diffusive segments when they are outside a cluster. Similar phenomena are observed in sphere dimer simulations and are likely to be responsible for the behavior observed in the intermediate regime.

V. SUMMARY AND CONCLUSION

As in many other active particle suspensions, systems containing many chemically powered self-propelled sphere dimer motors display collective motion including swarming of transient self-assembled clusters of motors. The transport properties differ from those of systems with a single dimer motor and the self-diffusion coefficient and orientational relaxation time depend in nontrivial ways on the number of dimers. The structural correlations that exist in the transient clusters depend on the dimer shape determined by the relative sizes of the catalytic and noncatalytic monomers in the sphere dimer motors.

A number of factors are responsible for the nature of the collective dynamics. The dimer motors considered in this investigation do not interact through cohesive intermolecular forces. The observed self-assembly can be understood in terms of the motions of the individual motors induced by their self-generated concentration gradients and that due to other motors in their neighborhoods. Hydrodynamic interactions are included in our investigations but interactions due to chemical gradients appear to play a more significant role in the dynamics than hydrodynamic coupling. For example, if hydrodynamic coupling is turned off, self-assembly of motors into transient clusters still occurs.

Applications may employ ensembles of motors to perform tasks such as targeted delivery of cargo to a given location. When many motors are launched to perform a task the interactions among the motors must be taken into account. The results presented in this paper indicate how such interactions influence the behavior and lead to active self-assembly, swarming, and distinctive correlations that depend on motor geometry. The active self-assembly process leading to coherent motion of collections of motors may provide an effective way to deliver large amounts of cargo to a specific location. Thus this work should aid in the design of protocols for applications involving the dynamics of many chemically powered nanomotors.

ACKNOWLEDGMENTS

The work of R.K. was supported in part by a grant from the Natural Sciences and Engineering Research Council of Canada. Computations were performed on the GPC supercomputer at the SciNet HPC Consortium [60]. SciNet is funded by the Canada Foundation for Innovation under the auspices of Compute Canada, the Government of Ontario, Ontario Research Fund–Research Excellence, and the University of Toronto. S.T. would like to acknowledge DST for financial support.

[1] N. J. Carter and R. A. Cross, Nature (London) **435**, 308 (2005).
[2] R. D. Vale and R. A. Milligan, Science **288**, 88 (2000).
[3] A. B. Kolomeisk and M. E. Fisher, Annu. Rev. Phys. Chem. **58**, 675 (2007).
[4] H. C. Berg, *E. coli in Motion* (Springer-Verlag, New York, 2004).
[5] E. M. Purcell, Am. J. Phys. **45**, 3 (1977).
[6] H. Ke, S. Ye, R. L. Carroll, and K. Showalter, J. Phys. Chem. A **114**, 5462 (2010).

[7] J. R. Howse, R. A. L. Jones, A. J. Ryan, T. Gough, R. Vafabakhsh, and R. Golestanian, Phys. Rev. Lett. **99**, 048102 (2007).
[8] W. F. Paxton *et al.*, J. Am. Chem. Soc. **126**, 13424 (2004).
[9] W. F. Paxton, A. Sen, and T. E. Mallouk, Chem. Eur. J. **11**, 6462 (2005).
[10] R. Golestanian, T. B. Liverpool, and A. Ajdari, New J. Phys. **9**, 126 (2007).
[11] L. Qin *et al.*, J. Am. Chem. Soc. **129**, 14870 (2007).
[12] G. A. Ozin, I. Manners, S. Fournier-Bidoz, and A. Arsenault, Adv. Mater. **17**, 3011 (2005).
[13] L. F. Valadares *et al.*, Small **6**, 565 (2010).
[14] G. Rückner and R. Kapral, Phys. Rev. Lett. **98**, 150603 (2007).
[15] Y.-G. Tao and R. Kapral, J. Chem. Phys. **128**, 164518 (2008).
[16] S. Thakur and R. Kapral, J. Chem. Phys. **133**, 204505 (2010).
[17] N. Mano and A. Heller, J. Am. Chem. Soc. **127**, 11574 (2005).
[18] W. A. Thompson, I. Vertinsky, and J. R. Krebs, J. Anim. Ecol. **43**, 785 (1974).
[19] T. J. Pitcher, B. L. Partridge, and C. S. Wardle, Science **194**, 963 (1976).
[20] T. Vicsek, A. Czirok, E. Ben-Jacob, I. Cohen, and O. Shochet, Phys. Rev. Lett. **75**, 1226 (1995).
[21] G. Grégoire and H. Chaté, Phys. Rev. Lett. **92**, 025702 (2004).
[22] H. Chaté, F. Ginelli, G. Grégoire, and F. Raynaud, Phys. Rev. E **77**, 046113 (2008).
[23] W. Ebeling and L. Schimansky-Geier, Eur. Phys. J. Special Topics **157**, 17 (2008).
[24] F. Ginelli, F. Peruani, M. Bär, and H. Chaté, Phys. Rev. Lett. **104**, 184502 (2010).
[25] J. Deseigne, O. Dauchot, and H. Chaté, Phys. Rev. Lett. **105**, 098001 (2010).
[26] R. A. Simha and S. Ramaswamy, Phys. Rev. Lett. **89**, 058101 (2002).
[27] D. Saintillan and M. J. Shelley, Phys. Rev. Lett. **100**, 178103 (2008).
[28] J. P. Hernandez-Ortiz, C. G. Stoltz, and M. D. Graham, Phys. Rev. Lett. **95**, 204501 (2005).
[29] J. P. Hernandez-Ortiz, P. T. Underhill, and M. D. Graham, J. Phys.: Condens. Matter **21**, 204107 (2009).
[30] J. Howard, *Mechanics of Motor Proteins and the Cytoskeleton* (Sinauer, Sunderland, MA, 2001).
[31] U. Börner, A. Deutsch, H. Reichenbach, and M. Bär, Phys. Rev. Lett. **89**, 078101 (2002).
[32] U. Börner, A. Deutsch, and M. Bär, Phys. Biol. **3**, 138 (2006).
[33] O. A. Igoshin, A. Goldbeter, D. Kaiser, and G. Oster, Proc. Natl. Acad. Sci. USA **101**, 15760 (2004).
[34] C. Dombrowski, L. Cisneros, S. Chatkaew, R. E. Goldstein, and J. O. Kessler, Phys. Rev. Lett. **93**, 098103 (2004).
[35] J. P. Hernandez-Ortiz, C. G. Stoltz, and M. D. Graham, Phys. Rev. Lett. **95**, 204501 (2005).
[36] D. B. Kearns, Nat. Rev. Microbiol. **8**, 634 (2010).
[37] H. P. Zhang *et al.*, Europhys. Lett. **87**, 48011 (2009).
[38] H. P. Zhang, A. Be'er, E.-L. Florin, and H. L. Swinney, Proc. Natl. Acad. Sci. USA **107**, 13626 (2010).
[39] S. Ebbens, R. A. L. Jones, A. J. Ryan, R. Golestanian, and J. R. Howse, Phys. Rev. E **82**, 015304 (2010).
[40] M. Ibele, T. E. Mallouk, and A. Sen, Angew. Chem. Int. Ed. **48**, 3308 (2009).
[41] C. M. Pooley, G. P. Alexander, and J. M. Yeomans, Phys. Rev. Lett. **99**, 228103 (2007).
[42] A. Najafi and R. Golestanian, Phys. Rev. E **69**, 062901 (2004).
[43] A. Kanevsky, M. J. Shelley, and A.-K. Tornberg, J. Comput. Phys. **229**, 958 (2010).
[44] Y.-G. Tao and R. Kapral, J. Chem. Phys. **131**, 024113 (2009).
[45] The z axis of the simulation box should not be confused with the unit vector $\hat{\mathbf{z}}$ along a dimer bond.
[46] Here we consider irreversible reactions but the simulations are easily generalized to treat reversible reactions driven out of equilibrium by fluxes of molecules.
[47] A. Malevanets and R. Kapral, J. Chem. Phys. **110**, 8605 (1999).
[48] A. Malevanets and R. Kapral, J. Chem. Phys. **112**, 72609 (2000).
[49] A. Malevanets and R. Kapral, Lect. Notes Phys. **640**, 116 (2004).
[50] R. Kapral, Adv. Chem. Phys. **140**, 89 (2008).
[51] G. Gompper, T. Ihle, D. M. Kroll, and R. G. Winkler, Adv. Polym. Sci. **221**, 1 (2009).
[52] S. H. Lee and R. Kapral, J. Chem. Phys. **122**, 214916 (2005).
[53] J. T. Padding and W. J. Briels, J. Chem. Phys. **132**, 054511 (2010).
[54] See Supplemental Material at http://link.aps.org/supplemental/10.1103/PhysRevE.85.026121 for movies of the dynamics of several dimer systems.
[55] R. Golestanian, Phys. Rev. Lett. **102**, 188305 (2009).
[56] J. Toner and Y. Tu, Phys. Rev. Lett. **75**, 4326 (1995).
[57] G. Grégoire, H. Chaté, and Y. Tu, Phys. Rev. Lett. **86**, 556 (2001).
[58] S. Ramaswamy, R. A. Simha, and J. Toner, Europhys. Lett. **62**, 196 (2003).
[59] X.-L. Wu and A. Libchaber, Phys. Rev. Lett. **84**, 3017 (2000).
[60] J. Dursi *et al.*, J. Phys.: Conf. Ser. **256**, 012026 (2010).